Available online at www.sciencedirect.com
ScienceDirect
Journal of Nuclear Materials 363–365 (2007) 1110–1118
journal of nuclear materials
www.elsevier.com/locate/jnucmat

Influence of boronization on operation with high-Z plasma facing components in Alcator C-Mod

B. Lipschultz [a,*], Y. Lin [a], E.S. Marmar [a], D.G. Whyte [b], S. Wukitch [a], I.H. Hutchinson [a], J. Irby [a], B. LaBombard [a], M.L. Reinke [a], J.L. Terry [a], G. Wright [b], The Alcator C-Mod Group

[a] *M.I.T. Plasma Science and Fusion Center, 175 Albany Street, Cambridge, MA 02139, USA*
[b] *University of Wisconsin-Madison, 1500 Engineering Drive, Madison, WI 53706, USA*

Abstract

We report the results of operation of Alcator C-Mod with all high-Z molybdenum plasma facing component (PFC) surfaces. Without boron-coated PFCs energy confinement was poor ($H_{ITER,89} \sim 1$) due to high core molybdenum ($n_{Mo}/n_e \leqslant 0.1\%$) and radiation. After applying boron coatings, n_{Mo}/n_e was reduced by a factor of 10–20 with $H_{ITER,89}$ approaching 2. Results of between-discharge boronization, localized at various major radii, point towards important molybdenum source regions being small, outside the divertor, and due to RF-sheath-rectification. Boronization also has a significant effect on the plasma startup phase lowering Z_{eff}, radiation, and lowering the runaway electron damage. The requirement of low-Z coatings over at least a fraction of the Mo PFCs in C-Mod for best performance together with the larger than expected D retention in Mo, give impetus for further high-Z PFC investigations to better predict the performance of un-coated tungsten surfaces in ITER and beyond.

PACS: 52.25.Vy; 52.55.Fa; 52.40.Hf; 52.25.Vy

Keywords: Boronization; Molybdenum; High-Z material; Erosion; Alcator C-Mod

1. Introduction

Studies of plasma facing component (PFC) candidate materials for a magnetic fusion reactor generally conclude that tungsten is currently the best choice due to its low tritium (T) solubility [1], capability to handle high heat fluxes with low erosion, and robustness to nuclear damage and activation [2–7]. Tungsten is being considered for all ITER PFCs [8] for the above advantages over carbon as well as to provide the necessary operational experience for a reactor. However, there is minimal published divertor tokamak data detailing experience with un-coated, 'pure', high-Z surfaces. This makes it difficult to ascertain whether the operational advantages of tungsten over carbon will hold true in a reactor environment. Alarmingly, ITER/reactor

* Corresponding author. Fax: +1 617 253 0627.
E-mail address: blip@psfc.mit.edu (B. Lipschultz).

0022-3115/$ - see front matter
doi:10.1016/j.jnucmat.2007.01.227

performance is based on a confinement database primarily derived from carbon PFC tokamaks (also using low-Z coatings). The question of whether such performance predictions would also hold with solely high-Z PFCs remains. Alcator C-Mod is well-placed to research such issues as it operates with all molybdenum (Mo) high-Z PFCs, which have very similar properties to tungsten in terms of erosion, T retention [9] and radiation in the core plasma (at C-Mod plasma temperatures). Boron coatings were removed from all C-Mod surfaces (tiles, vessel surfaces, support hardware) prior to the 2005 run period to provide a unique comparison of operation with or without boronized molybdenum PFCs in a diverted tokamak.

We have previously reported a general comparison of molybdenum PFC operation both with and without boron coatings [10]. ICRF-heated H-modes were readily achieved utilizing molybdenum PFCs without boron coatings although the resultant enhancement in energy confinement was typically small ($H_{\mathrm{ITER},89} \sim 1$). Core molybdenum concentrations, $n_{\mathrm{Mo}}/n_{\mathrm{e}}$, rose rapidly after the H-mode transition, cooling the plasma by line radiation which reduces the edge pedestal height. This leads to a reduction in energy confinement. D retention after a single shot, both prior to boronization and post-boronization, was higher than expected based on laboratory ion-beam studies [11]. The D retention rate is reduced when integrated over a longer period – days, weeks or even a run period due to D release from surfaces that are heated by plasma disruptions. Long-term D retention is currently being studied both in C-Mod and in related laboratory experiments. Boron coatings lowered core molybdenum levels by a factor of 10–20 leading to strong reductions in core radiated power and increasing $H_{\mathrm{ITER},89}$ up to ~2. The effects of each overnight boronization are found to be limited in time to 10 s of RF-heated H-mode discharges, correlated to time-integrated RF-input energy. Intra- and inter-discharge boronization techniques were reported with the latter being the most successful.

In this paper we report on further experiments aimed at understanding what leads to the rapid loss of boronization layers and what can be done to improve solely high-Z PFC operation. The emphasis here will be on determining where the most important Mo erosion locations affecting the plasma are, their size, and the erosion mechanism. A companion paper more specifically explores the Alcator C-Mod experience of ICRF operation in a high-density, high-Z PFC, divertor tokamak environment [12].

2. General experiment description

The general characteristics of the C-Mod device as well as SOL and divertor physics research are reported in more depth elsewhere [13–15]. The results reported in this paper are from lower single-null plasmas. The H-mode plasmas are both Ohmic (1.2 MA) and ICRF-heated (1.0 MA, H-minority), all with toroidal fields of 5.3 T. A typical plasma equilibrium and surrounding PFC surfaces are shown in Fig. 1.

Alcator C-Mod applies boronization to surfaces differently than most other tokamaks. The C-Mod boronization procedure employs an electron cyclotron discharge cleaning (ECDC) plasma discharge with a helium–diborane gas mixture (typically 10% B_2D_6, 90% He). The plasma is created at the major radius where the electron cyclotron frequency microwaves ($f = 2.45$ GHz) are resonant with the toroidal magnetic field which is varied to sweep the resonance across the chamber [$0.059 \leqslant B_{\mathrm{T}}$ (on axis) $\leqslant 0.13$ T]. The plasma characteristics are not uniform in major radius linked to the resonance location [16]. Toroidal uniformity is maintained by releasing the diborane gas into the vessel from a toroidal pipe located at the top of the vessel with holes spaced ~1 cm toroidally. The overnight boronization period is ~12 h resulting in a coating thickness ~150–200 nm assuming uniform deposition over a 10 m^2 area. The thickness of the overnight boronization layer appears to be fairly uniform poloidally as well based on the tile surface analysis performed on a set of tiles removed from the tokamak after 7 years of operation, Fig. 2. The layer thickness is typically ~5 μm at most poloidal locations except at regions of the outer divertor that receive large power and particle fluxes. Thinner layers are found at the inner divertor because those tiles were installed for a shorter period.

When utilized for between-discharge boronization, the boronization period is shortened to periods in the range 10–20 min. The resonance region is usually swept over a fraction of the vessel major radius range for these depositions as a method of identifying where the most important boron erosion regions are located. The deposition is correlated with the resonance location. However, we are quite sure that some fraction of the deposition, yet to be properly quantified, is outside the resonance region.

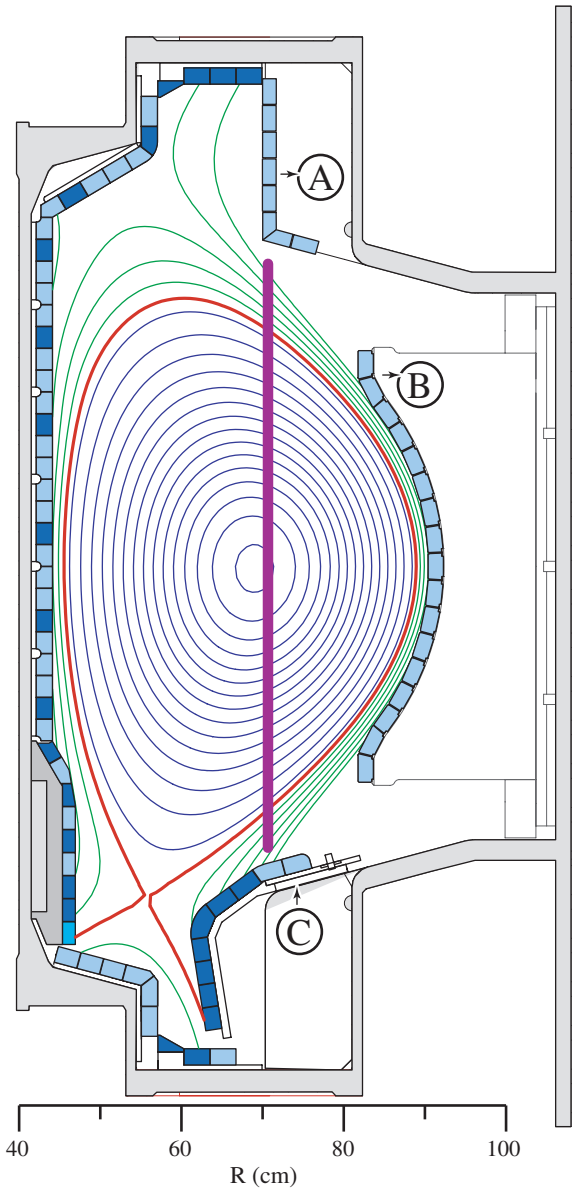

Fig. 1. Alcator C-Mod vessel. Locations (A), (B) and (C) refer respectively to the upper gusset protection tiles, the outer limiter and the top of the outer divertor. The vertical line corresponds to $R = 70$ cm. The poloidal location of tiles removed for surface analysis prior to the 2005 campaign are darkened.

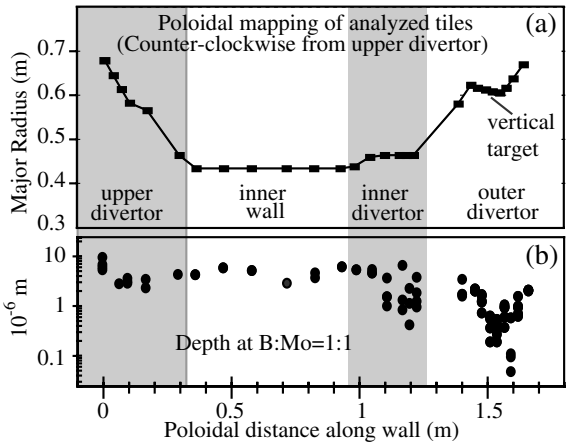

Fig. 2. (a) Poloidal map of analyzed Mo tiles; (b) effective boron layer thickness on Mo tiles shown as the depth from surface at which the B:Mo ratio is 1:1 as determined by proton (2500 keV) Rutherford backscattering spectroscopy. Multiple data points at a single poloidal location correspond to multiple measurement locations on the same tile.

3. Plasma performance with and without boronized PFC surfaces

The plasmas described herein are generally described as 'pre-boronization' or 'post-boronization'. By the former we are referring to that part of a run period following a vacuum break where all surfaces in the vessel have been wiped clean of boron. In practice all boron cannot be removed. The amount of boron remaining on tiles was very low as determined from nuclear reaction analysis measurements [10]: 10–30% B/Mo distributed through the first micron, either trapped in the topography of the surface or in grain boundaries. In any case the cleaned tile surfaces had predominately Mo at the surface, a stark difference to the large thickness (typically in the range of 6–10 μm) of boron that had accumulated over years of operation [10] with 1% Mo surface average. 'Post-boronization' then refers to operation after at least one overnight boronization as described above.

As reviewed in the introduction the difference between pre- and post-boronization is stark. The waveforms for two discharges illustrative of the pre- and post-boronization periods are shown in Fig. 3. The pre-boronization discharge transitioned to H-mode with a rapid increase in density and radiation. An equilibrium was then reached with marginally improved particle confinement, as evidenced by the very small increase to the final H-mode density and poor energy confinement. The post-boronization discharge that is shown has much lower radiated power and core Mo density accompanying much better energy confinement.

Analysis of the plasma profiles has shown a clear correlation between degraded energy confinement and increased central radiation fractions. This is thought to be due to local cooling of the pedestal

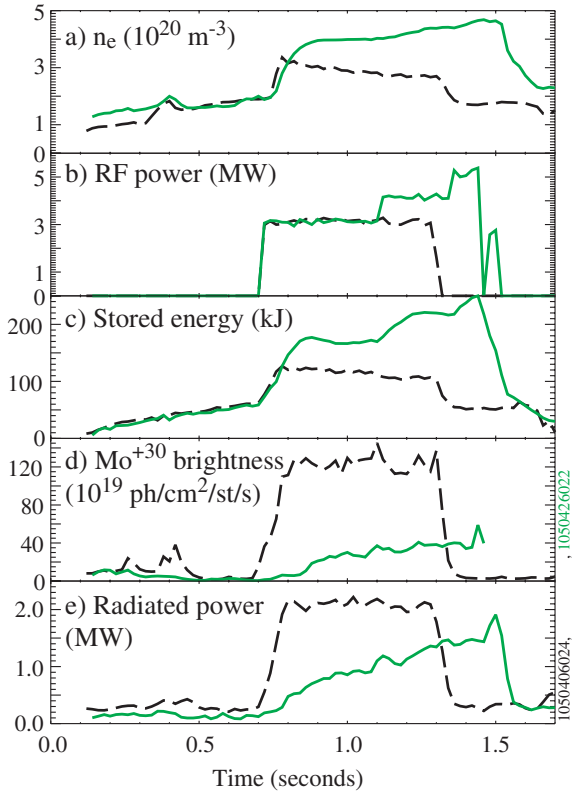

Fig. 3. A set of characteristic traces from pre- (---) and post-boronization (—) discharges.

by Mo radiation (the dominant radiator in C-Mod) which lowers the H-mode pedestal plasma pressure that, through profile stiffness, leads to lower plasma pressures in the core and decreases in the overall stored energy [10].

4. Localized erosion of B coatings

A number of results point towards localized erosion of the boronization layer. The clearest evidence is that prior to cleaning the vessel surfaces of boron a poloidal array of tiles were removed from the machine and analyzed using high-energy ion-beam surface analysis (RBS, NRA) techniques. Boron layers in the range of 6 μm thick were generally found on all tiles except for the outer and inner divertor tiles (Fig. 2). The 6 μm thickness corresponds to integration of multiple boronization layers over 6–7 years of operation. The boron layers have not been eroded from the majority of PFC surfaces and typically contain ~1% Mo and lesser amounts of other impurities (O, C, Ar) in the near surface (<0.1 μm). The outer divertor surfaces showed the highest Mo surface concentrations (10–50%), presumably due to net erosion of the boron layers by the high particle and heat fluxes to those surfaces. These regions of 'plasma-cleaned' surfaces extend from the bottom of the outer divertor vertical section to $R \sim 0.67$ m (see Figs. 1 and 2). The boron thickness is also thinner than 6 μm for tiles on the uppermost section of the outer divertor (Figs. 1(C) and 2).

Visual inspection of the entire vessel leads to identification of additional regions of eroded boron that are toroidally localized. These include most of the surfaces of the two poloidal limiters located at the outboard edge of the plasma (Fig. 1(B)). Vessel protection tiles located on gussets (24 – 1 cm thick – plates spaced toroidally, see Fig. 1(A)) used to strengthen the vessel were also fairly clean of boron. The leading edges of the ten outer divertor modules, which are known to receive disproportionate heat loads compared to other divertor tiles, are also generally free of boron. We also suspect that the leading edges of many of the outer divertor tiles even far from the strike point are free of boron. All front surfaces of the tiles are chamfered at the toroidal leading edges to make sure no field line impacts the side of the tile. As a result the heat/particle fluxes are not uniform toroidally across the front surface. The edges of the front surface of each tile will likely have higher erosion rates.

Experiments aimed at determining the poloidal region of the most important molybdenum impurity source affecting the core plasma have also been successful. Previous studies [10] utilized between-discharge boronization (BDB) by sweeping the resonance over a 10 cm region. The experimental sequence followed the application of BDB by repeated tokamak discharges to determine how long the coating effects lasted. The center of the boronization sweep was then varied from one BDB sequence to the next to determine whether there were particular radial locations where the boronization was more effective. The results of this scan, reproduced in Fig. 4, show that the radiation at the transition to the H-mode was lowest when the BDB center was located at $R = 70$ cm. This location corresponds to both the top of the outer divertor and to the upper gusset tiles (see Fig. 1(A)). That the most effective BDB location is outside the divertor is consistent with other results: increases in source rates outside the divertor derived from Mo I brightnesses have been shown to be best correlated with increases in core Mo levels [17]; injection of N_2

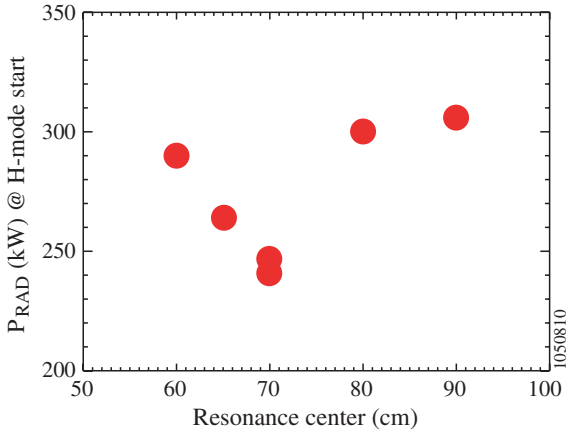

Fig. 4. The radiated power in ICRF-heated L-mode plasmas just prior to the transition to H-mode is plotted as a function of the resonance location for discharges following between-discharge boronization.

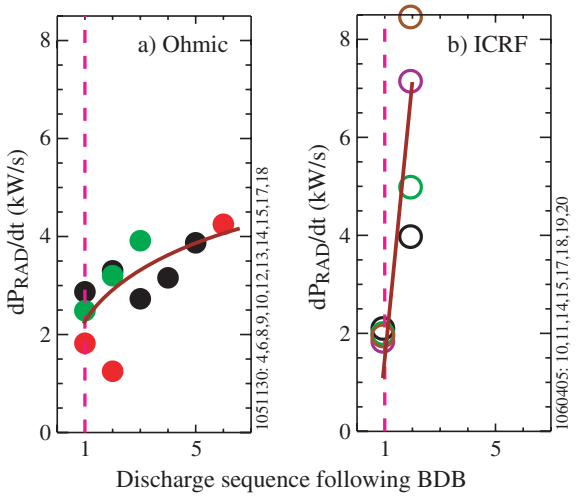

Fig. 5. A comparison of the rate of radiation increase at the start of an H-mode for sequences of discharges following a between-discharge boronization. Each sequence corresponds to one color: (a) Ohmic H-modes and (b) ICRF-heated H-modes.

into the divertor lowered the Mo source rate near the outer strike point (vertical target region) without affecting core molybdenum levels [10]; the probability of impurities reaching the core plasma when launched from outside the divertor on the outboard side is much higher (×100) than for impurities launched from the divertor [18,17].

5. Role of ICRF in eroding boronization layers

We have also used the BDB technique as a diagnostic tool to explore the role of the ICRF in eroding the boron and molybdenum. Fig. 5 displays the rate of increase of radiated power at the beginning of an H-mode for a number of BDB discharge sequences for both Ohmic and RF-heated H-modes. Each sequence consists of the BDB followed by 2–6 discharges (without BDB). The Ohmic discharges were programmed at higher current so that the discharge-integrated input energy (2.7 MJ) was similar to that of RF-heated discharges (3.2 MJ). For Ohmic H-modes the rate of radiation increase stays low for 4–6 discharges following BDB. In contrast, for RF-heated H-modes, we see that the rate of radiation increase at the start of the H-mode (dP_{RAD}/dt) is much higher after the first discharge in the sequence. This behavior is reflected in the degradation of the energy confinement in these discharges which was similar at the start of each sequence but degraded as the sequence proceeded and the Mo influx increased. The degradation in confinement was much faster for the ICRF-heated discharge. We infer that the ICRF waves are eroding the boron layer faster than for Ohmic discharges. We have not performed any experiments to determine where the most important erosion locations are for Ohmic plasmas.

Assuming that the RF antennas are leading to localized erosion then the likely mechanism discussed previously [17], is RF-sheath-rectification. The enhancement of the sheath voltage is likely occurring on flux tubes that intersect with, or pass in front of, the antenna. We have traced the toroidal and poloidal trajectory of all such flux tubes, following them to their termination on non-antenna PFC surfaces [12]. Most flux tubes impact the main limiters, upper gusset tiles, or the top of the outer divertor (Fig. 1). Since the D/E port antennas are displaced toroidally from the J antenna (180° toroidally from D to J ports) the corresponding erosion location will be displaced toroidally as well. This hypothesis was confirmed by the lack of performance degradation when sequential discharges rely on different antennas for heating [12]. The erosion can be linked to a specific antenna and that the erosion due to each antenna is toroidally displaced from the other. The erosion in this area correlates with the thinner B layers found on the uppermost surfaces of the outer divertor (Fig. 2). However, a previous tile analysis did not show significantly thinner B layers [19].

The localized erosion by specific antennas is also supported by other measurements. Both IR camera

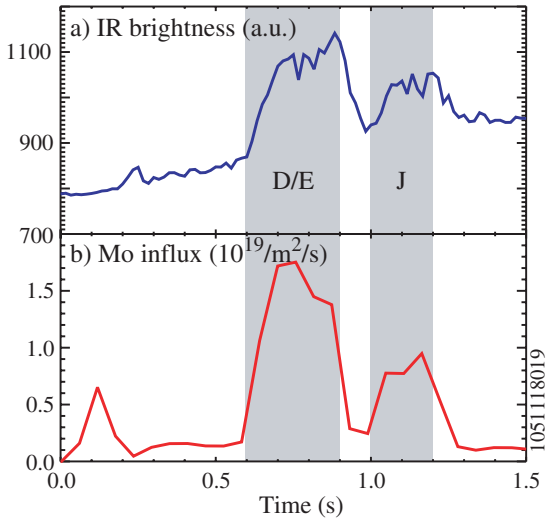

Fig. 6. Diagnostic measurements viewing the surface of the top of the outer divertor cover plate (Fig. 1(C)): (a) the IR brightness and (b) Mo influx determined from Mo I at 386.4 nm.

(only an approximate calibration for conversion to surface temperature available) and visible spectroscopic (Mo influx) diagnostics view the top of the outer divertor ($R \sim 70$ cm) region that maps along field lines to the D/E antenna for the equilibria utilized in these studies. During the period when the D/E antennas are launching power those diagnostics show a small temperature rise (not found elsewhere on the divertor plate) and a corresponding Mo influx (see Fig. 6).

6. Modelling of localized erosion

The hypothesis both of erosion linked to the ICRF heating and its localization in small PFC regions outside the high heat flux section of the divertor is supported by simple modelling of sputtering rates. This is not meant as a detailed model but more as a rough check on whether the hypothesis is realistic. There are two primary pieces of information that are utilized in this model: (1) the *net* boron erosion rate is estimated based on the observation that the B coating due to between-discharge boronization (~15 nm) erodes over a period of ~0.5 s of RF power. This corresponds to $\Gamma_B \sim 4 \times 10^{21}$ B/m^2/s; (2) the *gross* Mo influx rate can be estimated from a typical n_{Mo}/n_e level of 10^{-4} in H-mode, a core electron density of 4×10^{20} m^{-3}, and an impurity confinement time of 0.1 s [20] to be $\Gamma_{Mo} \sim 4 \times 10^{17}$ s^{-1}. Since the impurity penetration probability through the outer SOL is typically ~0.1 in C-Mod [18,17] the total influx required from surfaces is then 4×10^{18} s^{-1}. If we assume that the same incident species flux mixture and characteristics contribute to the erosion of the B, and subsequently of the underlying molybdenum, then we can write down the following equations:

$$\Gamma_D(Y_{B,D} + \eta_B \cdot Y_{B,B})/\gamma = \Gamma_B = 4 \times 10^{21}\,/\mathrm{m}^2\,/\mathrm{s},$$
$$\Gamma_D(Y_{Mo,D} + \eta_B \cdot Y_{Mo,B}) \cdot A = \Gamma_{Mo} \cdot A \approx 4 \times 10^{18}\,/\mathrm{s}, \quad (1)$$

where η_B is the boron fraction, n_B/n_e, Γ_D is the perpendicular ion flux, A is the area of the affected region, $Y_{B,B}$ and $Y_{B,D}$ are the sputtering rates respectively for B^{+3} on boron (based on previous work [17]) and D^+ on boron, and $Y_{Mo,B}$ and $Y_{Mo,D}$ are the sputtering rates for B^{+3} on Mo and D^+ on Mo. Γ_{Mo} and Γ_B are the net flux of those atoms leaving the surface after local redeposition. We have also allowed for the possibility that some of the eroded boron is redeposited by including the factor $\gamma > 1$. Such a factor is not included here for Mo because we infer the gross Mo source rate (as opposed to the net B erosion rate) from core measurements of the Mo density as described above. The 'transformation' from n_{Mo}/n_e to Γ_{Mo} is based on the gross erosion, or injection, source rate. Further defining a $Y_{eff,X} = Y_{X,D} + \eta_B \cdot Y_{X,B}$ we then find:

$$A(m^2) \times \frac{\gamma Y_{eff,Mo}}{Y_{eff,B}} = \frac{4 \times 10^{18}\,/\mathrm{s}}{4 \times 10^{21}\,/\mathrm{m}^2\,/s} \sim 10^{-3} \quad \text{or}$$
$$A(m^2) \sim 10^{-3} \cdot \frac{Y_{eff,B}}{\gamma Y_{eff,Mo}}. \quad (2)$$

For each value of the sheath voltage, we calculate the area and density (through Γ_D in Eq. (1)) required to satisfy the above equations. The heat flux and local surface temperature rise can be calculated as an additional check to see if the heat fluxes are reasonable. For the situation where the incident flux is due to sheath-rectified ions then the incident ion energy, E_{ION}, used to calculate the sputtering rates is $E_{ION} = Z_{ION} * V_{sheath} + 2.0 * E_{Thermal}$. Z_{ION} is the ionization state of the impacting ion and V_{Sheath} the rectified sheath voltage which was previously found to be in the range 100–400 V on field lines connected to the active antenna [17]. T_i is assumed equal to T_e (~10 eV in the far SOL) for calculation of $E_{Thermal}$. For the purposes of this discussion $\gamma \sim 1$ since the result is linear in γ. Because the erosion location corresponds to the far SOL we assume that the sputtered Mo and B

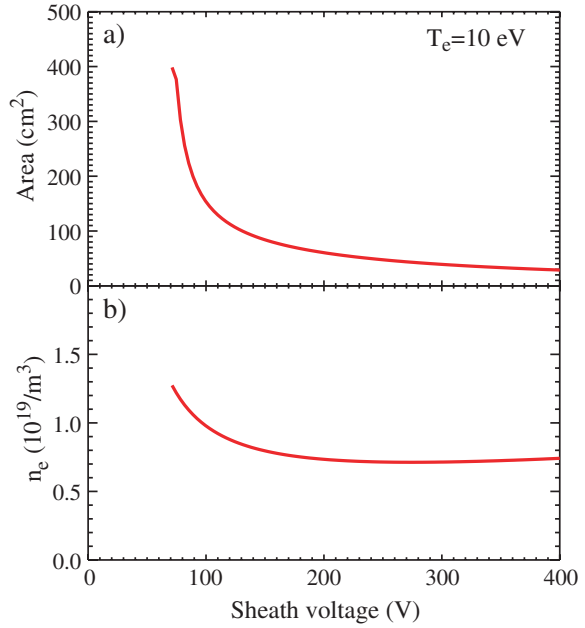

Fig. 7. The calculated characteristics of the surface area (a) affected by ions accelerated through a sheath enhanced by the RF and (b) plasma density of the thermal plasma. Thermal plasma temperature of 10 eV assumed.

that are ionized do not immediately return to the same region to self-sputter and so have not included such an effect. Fig. 7 displays the results of the analysis for both the area affected and plasma density on the flux tube impacting it. B^{+3} ion sputtering dominates the erosion of both Mo and B. Over almost the entire energy range shown, the required area (Fig. 7(a)) is very small, 30–130 cm^2, 0.05–0.2% of the total Mo PFC area (~7 m^2). The density on the flux tube (Fig. 7(b)) is inferred to be below 10^{19} m^{-3} which is not uncommon at, or beyond, the limiter radius in C-Mod. Note that allowing $\gamma_{Mo}/\gamma_B > 1$ lowers the area while raising the density. The corresponding temperature rise for surfaces on the top of the outer divertor would be small (10–50 °C) consistent with the IR measurements.

7. Effect of boronization on plasma startup

A rarely discussed, but important part of the discharge, is the startup period. This period is particularly important for ITER. Volt–second consumption during startup should be minimized requiring low impurity levels. Damage to startup limiters from runaway electrons is also a concern.

Boronization of PFC surfaces has important effects on a number of plasma characteristics during the C-mod discharge startup phase. This phase lasts ~250 ms during which the plasma is limited on the inner wall and much of the final plasma current and density are achieved. Fig. 8 displays the radiated power and Z_{eff}, averaged over the period 0.125–0.25 s, for a sequence of discharges from the beginning of the 2005 run period through two overnight boronizations. Prior to the first boronization, when PFC surfaces are un-coated and the RF power (during the diverted phase of the discharge) increased, the radiated power and Z_{eff} both rose over time. Mo and Fe are the dominant radiators and probably dominate Z_{eff} as well. Both the radiated power and Z_{eff} drop after the first (and second) boronization and stay low. We have not determined the primary radiating species during startup for that period.

The drop in radiated power during plasma startup post-boronization leads to enhancements in other aspects of machine operation. Fig. 9 displays the hard-X-ray signal during startup for a set of discharges pre- and post-boronization as a function of the plasma density normalized to the Greenwald density limit [21]. The higher radiation and resistivity occurring in pre-boronization discharges necessitates lowering the maximum allowable startup density ($P_{RAD} \sim n_e^2$); Later in the discharge the runaway electrons that are engendered

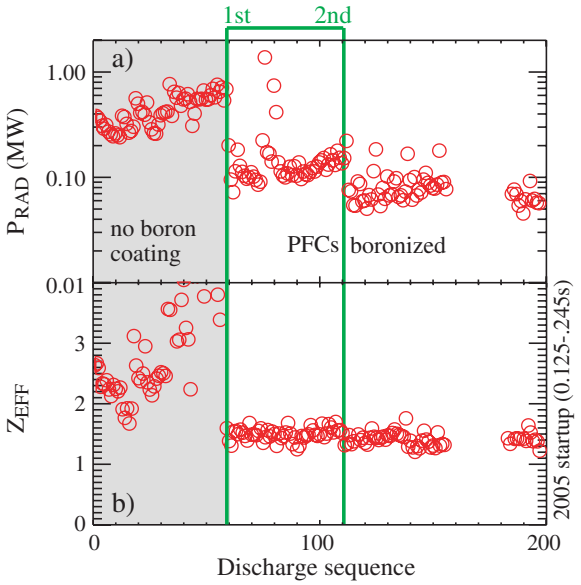

Fig. 8. Discharge sequence showing the variation of the radiated power (a) and Z_{eff} (b) during the 2005 run campaign. Both pre- and post-boronization periods are shown. Vertical lines and 'B' connote occurrence of an overnight boronization.

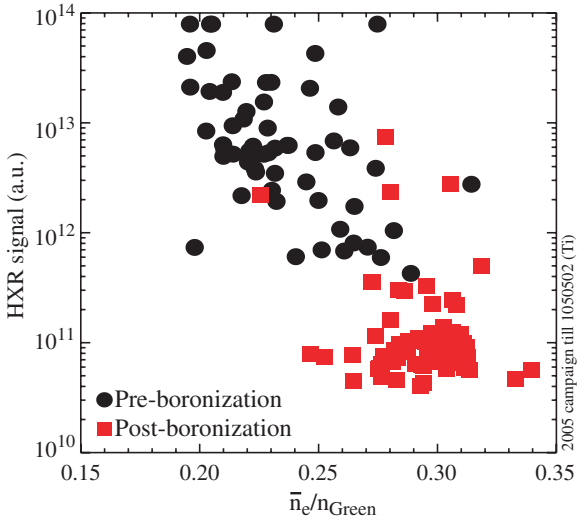

Fig. 9. Hard-X-ray signal as a function of the line-averaged density normalized to the Greenwald density for the same pre- and post-boronization periods.

by the low-density, high Z_{eff} and loop voltage, impact the outer limiter leading to hard-X-rays and melting of Mo PFCs. Fig. 9 also shows that after boronization the startup density can be raised and the hard-X-rays and runaway electrons disappear except for cases when the density is intentionally kept low.

8. Implications for ITER and reactors

The results discussed above have mixed implications regarding high-Z PFC operation in ITER and beyond. In general operation with all high-Z PFCs and without boronization is problematic for achieving the best performance. However initial ITER operation is currently planned with a mixture of low- and high-Z materials. The Be main chamber wall may act like boronization in that eroded Be will tend to coat other surfaces around the chamber with a low-Z material. Such Be coatings will likely develop on low erosion PFC surfaces leading to the long-term beneficial effects of the first boronization in C-Mod that lowers the background level of Fe and other impurities. On the other hand, the ITER tungsten PFC surfaces are in a location geometrically similar to the top of the outer divertor plate in C-Mod. That geometry, together with the ICRF heating, creates the potential for strong sheath acceleration of ions into such W surfaces leading to localized areas of strong erosion, not amenable to coating by the Be. It is our opinion that the probability of the resultant impurities penetrating through the ITER outer SOL could be similar to that of C-Mod [22]. ELMs would also lead to an impurity source beyond that experienced in C-Mod that is poorly screened. ASDEX-Upgrade results with the partial high-Z tungsten tile coverage appear more encouraging than that from C-Mod [23,24]. Although the boronization layer has not been removed from ASDEX-Upgrade PFC surfaces each addition of more W PFC coverage has not been accompanied by difficulties achieving good confinement. We look forward to results from operation of ASDEX-Upgrade with ICRF and fully-W PFCs with the boron and carbon removed.

The current boronization techniques are not ideal for ITER. Coatings required to last through an entire ITER pulse are too thick (take too long, cost too much). Localized methods for B deposition both during and between discharges are one possible solution. Alternatively low-Z PFCs could be located in small regions of high-sheath voltage induced erosion leading to benign radiation.

C-Mod results raise the possibility that boronization may also be applicable to ITER for more long-term suppression of impurities in low plasma fluence areas. While boronization only has a short-term effect on the molybdenum in C-Mod discharges, it has a more long-term effect on general surfaces and impurities around the vessel, both for startup and performance phases of the discharge.

As ITER moves beyond mixed materials to all-tungsten PFCs the issues we describe above could further compromise operation if not better understood. Thus, for ITER and DEMO it is imperative that experiments on as many tokamaks as possible be addressing the issues of high-Z PFCs including erosion, impurity sources, impurity transport and D/T retention.

Acknowledgement

The authors would like to thank the excellent engineers, technical staff, students and scientists on the Alcator team for their support in this investigation. This work is supported by the US Department of Energy Cooperative Agreement No. DE-FC02-99ER54512.

References

[1] R. Causey, K. Wilson, T. Venhaus, W.R. Wampler, J. Nucl. Mater. 266–269 (1999) 467.

[2] C.H. Wu, J.P. Bonal, H. Kwast, F. Moons, G. Pott, H. Werle, G. Vieider, Fusion Eng. Des. 39&40 (1998) 263.
[3] V. Barabash, G. Federici, M.L. Rödig, L. Snead, C.H. Wu, J. Nucl. Mater. 283–287 (2000) 138.
[4] G. Federici, J.N. Brooks, D.P. Coster, et al., J. Nucl. Mater. 290–293 (2001) 260.
[5] H. Bolt, V. Barabash, G. Federici, J. Linke, A. Loarte, J. Roth, K.N. Sato, J. Nucl. Mater. 307–311 (2002) 43.
[6] V. Barabash, G. Federici, J. Linke, C.H. Wu, J. Nucl. Mater. 313–316 (2003) 42.
[7] M. Gasparotto, R. Andreani, L.V. Boccaccini, et al., Fusion Eng. Des. 66–68 (2003) 129.
[8] ITER Physics Expert group on divertor, ITER Physics Expert group on divertor modelling and database, and ITER Physics Basis Editors, Nucl. Fusion 39 (1999) 2391.
[9] A.A. Haasz, J.W. Davis, J. Nucl. Mater. 241–243 (1997) 1076.
[10] B. Lipschultz, Y. Lin, M.L. Reinke, et al., Phys. Plasmas 13 (2006) 056117.
[11] G.M. Wright, D.G. Whyte, B. Lipschultz, R. Doerner, J.G. Kulpin, J. Nucl. Mater., doi:10.1016/j.jnucmat.2007.01.135.
[12] S. Wukitch, B. Lipschultz, et al., J. Nucl. Mater., doi:10.1016/j.jnucmat.2007.01.273.
[13] I.H. Hutchinson, R. Boivin, F. Bombarda, et al., Phys. Plasmas 1 (1994) 1511.
[14] B. Lipschultz, B. LaBombard, S. Lisgo, J.L. Terry, Fusion Sci. Technol. 51 (2007) 390.
[15] B. Lipschultz, B. LaBombard, J.L. Terry, C.J. Boswell, I.H. Hutchinson, Fusion Sci. Technol. 51 (2007) 369.
[16] R.T. Nachtrieb, B.L. LaBombard, J.L. Terry, J.C. Reardon, W.L. Rowan, W.R. Wampler, J. Nucl. Mater. 266 (1999) 896.
[17] B. Lipschultz, D.A. Pappas, B. LaBombard, J.E. Rice, D. Smith, S.J. Wukitch, Nucl. Fusion 41 (2001) 585.
[18] G.M. McCracken, B. Lipschultz, B. Labombard, et al., Phys. Plasmas 4 (1997) 1681.
[19] W.R. Wampler, B. LaBombard, B. Lipschultz, G.M. McCracken, D.A. Pappas, C.S. Pitcher, J. Nucl. Mater. 266–269 (1999) 217.
[20] J.E. Rice, J.L. Terry, J.A. Goetz, et al., Phys. Plasmas 4 (1997) 1605.
[21] M. Greenwald, R.L. Boivin, F. Bombarda, et al., Nucl. Fusion 37 (1997) 793.
[22] B. Lipschultz, P. Andrew, J. Coad, et al.Proceedings of the 30th European Conference on Controlled Fusion and Plasma Physics, St. Petersburg, Russia, 7–11 July 2003, vol. 27A, European Physical Society, Geneva, 2003, p. 3.197.
[23] R. Neu, R. Dux, A. Geier, et al., Plasma Phys. Control. Fus. 44 (2002) 811.
[24] A. Kallenbach, R. Neu, R. Dux, et al., Plasma Phys. Control. Fus. 47 (2005) B207.